



Geochemistry of tourmalines associated with iron formation and quartz veins of the Morro da Pedra Preta Formation, Serra do Itaberaba Group (São Paulo, Brazil)

GIANNA M. GARDA¹, PAULO BELJAVSKIS², CAETANO JULIANI³ and DAILTO SILVA⁴

¹Departamento de Geologia Sedimentar e Ambiental, IGc-USP, 05508-080 São Paulo, SP, Brasil

²Programa de Recursos Minerais da Pós-Graduação, IGc-USP, 05508-080 São Paulo, SP, Brasil

³Departamento de Mineralogia e Geotectônica, IGc-USP, 05508-080 São Paulo, SP, Brasil

⁴Departamento de Metalogênese e Geoquímica, IGe-UNICAMP

Cx. Postal 6152, 13083-970 Campinas, SP, Brasil

Manuscript received on January 23, 2002; accepted for publication on March 7, 2003;

presented by JOSÉ MOACYR V. COUTINHO

ABSTRACT

Tourmalines of intermediate schorl-dravite composition occur in iron formation (including metachert and tourmalinites), metasediments, calc-silicate and metabasic/intermediate rocks of the Morro da Pedra Preta Formation, a volcanic-sedimentary sequence of the Serra do Itaberaba Group (northeast of São Paulo City, southeastern Brazil).

The Morro da Pedra Preta Formation is crosscut by quartz veins that contain both intermediate schorl-dravite and an alkali-deficient, Cr-(V)-bearing tourmaline, in which the occupancy of the X-site is $\square_{0.51}\text{Ca}_{0.33}\text{Na}_{0.15}$, characterizing it as intermediate to foitite and magnesiofoitite end-members. Mg# values for this tourmaline are higher than those for intermediate schorl-dravite.

Raman spectroscopy also confirms the presence of two groups of tourmalines. Stable isotope data indicate sediment waters as fluid sources, rather than fluids from magmatic/post-magmatic sources. $\Delta^{18}\text{O}$ compositions for tourmalines, host metachert, and quartz veins are similar, showing that fluid equilibration occurred during crystallization of both quartz and tourmaline.

Syngenetic, intermediate schorl-dravite tourmalines were formed under submarine, sedimentary-exhalative conditions; amphibolite-grade metamorphism did not strongly affect their compositions. Younger tourmalines of compositions intermediate to foitite and magnesiofoitite reflect the composition of the host rocks of quartz veins, due to fluid percolation along faults and fractures that caused leaching of Cr (and V) and the crystallization of these alkali-deficient, Cr-(V)-bearing tourmalines.

Key words: schorl-dravite series, foitite-magnesiofoitite, Serra do Itaberaba Group, Morro da Pedra Preta Formation.

INTRODUCTION

“The tourmaline minerals in all their aspects” was the topic of the meeting called “Tourmaline

Correspondence to: Gianna M. Garda
E-mail: giagarda@usp.br

1997", held in the Czech Republic in June 1997. Frank C. Hawthorne and Darrell J. Henry presented a proposal for classification of minerals of the tourmaline group, including the alkali-deficient tourmaline foitite (McDonald et al. 1993) among the thirteen valid end-members. The classification is based on chemical composition and ordering at the different crystallographic sites of the tourmaline structure (Hawthorne and Henry 1999).

The importance of tourmaline as a petrogenetic indicator has been pointed out by several authors (e.g. Henry and Guidotti 1985, Plimer 1986, 1988, Yavuz 1997) for its ample occurrence as an authigenic mineral in sedimentary and metamorphic rocks. In exploration, dravitic tourmalines have been associated with massive sulfide deposits and exhalites (Plimer 1986, 1987, 1988, Slack 1982, 1996, Slack et al. 1984, Taylor and Slack 1984, Willner 1992); schorlitic compositions have been associated with plutonic rocks (Taylor and Slack 1984), and exhalites (Plimer 1983), and alkali-deficient tourmalines with several environments (Hawthorne et al. 1999).

Tourmaline is a common mineral in the Serra do Itaberaba Group (State of São Paulo, southeastern Brazil), particularly in the basal volcanic-sedimentary sequence named Morro da Pedra Preta Formation (Juliani 1993), which was explored for gold in the 16th and 17th centuries.

Scanning electron microscopy revealed gold disseminated in tourmalinites and associated rocks in the Tapera Grande prospect, and alkali-deficient tourmalines associated with mineralized and barren quartz veins in the Quartzito prospect, both areas found in the Morro da Pedra Preta Formation. Distinct mineralization assemblages charac-

terize each area, with gold - pyrite - pyrrhotite-chalcopyrite in Tapera Grande (Beljavskis et al. 1999b) and electrum - pyrite - chalcopyrite-sphalerite - galena - scheelite - molybdenite in Quartzito (Garda et al. 1999).

The association of distinct tourmaline compositions with distinct types of mineralization in the Morro da Pedra Preta Formation led the authors to further investigate the subject, once rock-forming minerals such as amphibole, garnet, staurolite, and sillimanite (among others) proved to be useful for petrogenetic studies of the Serra do Itaberaba Group, but not specifically for mineralization.

THE SERRA DO ITABERABA GROUP

Three units compose the Serra do Itaberaba Group (Juliani 1993, Juliani and Beljavskis 1995): the Morro da Pedra Preta, Nhanguçu and Pirucaia Formations.

Lithostratigraphic and chemical characteristics indicate that the deposition of the basal Morro da Pedra Preta Formation began in an ensialic rift that evolved into a deep oceanic basin during the Mesoproterozoic (Juliani et al. 2000). A pile of basic rocks was generated at mid-ocean ridge segments, whereas sediments were deposited in a pelagic environment, with contribution of distal turbidites. Among the rock types, volcanic and volcanoclastic rocks, Algoma-type iron formation, and calc-silicate rocks are recognized. Sulfidation and gold deposition resulted from hydrothermal alteration related to the intrusion of andesitic and dacitic bodies in the volcano-sedimentary sequence under backarc regime (Garda et al. 2002, in press).

The deposition of the Nhanguçu Formation (manganiferous pelites and calc-pelites; carbonatic /calc-silicate rocks, rare (meta)basites

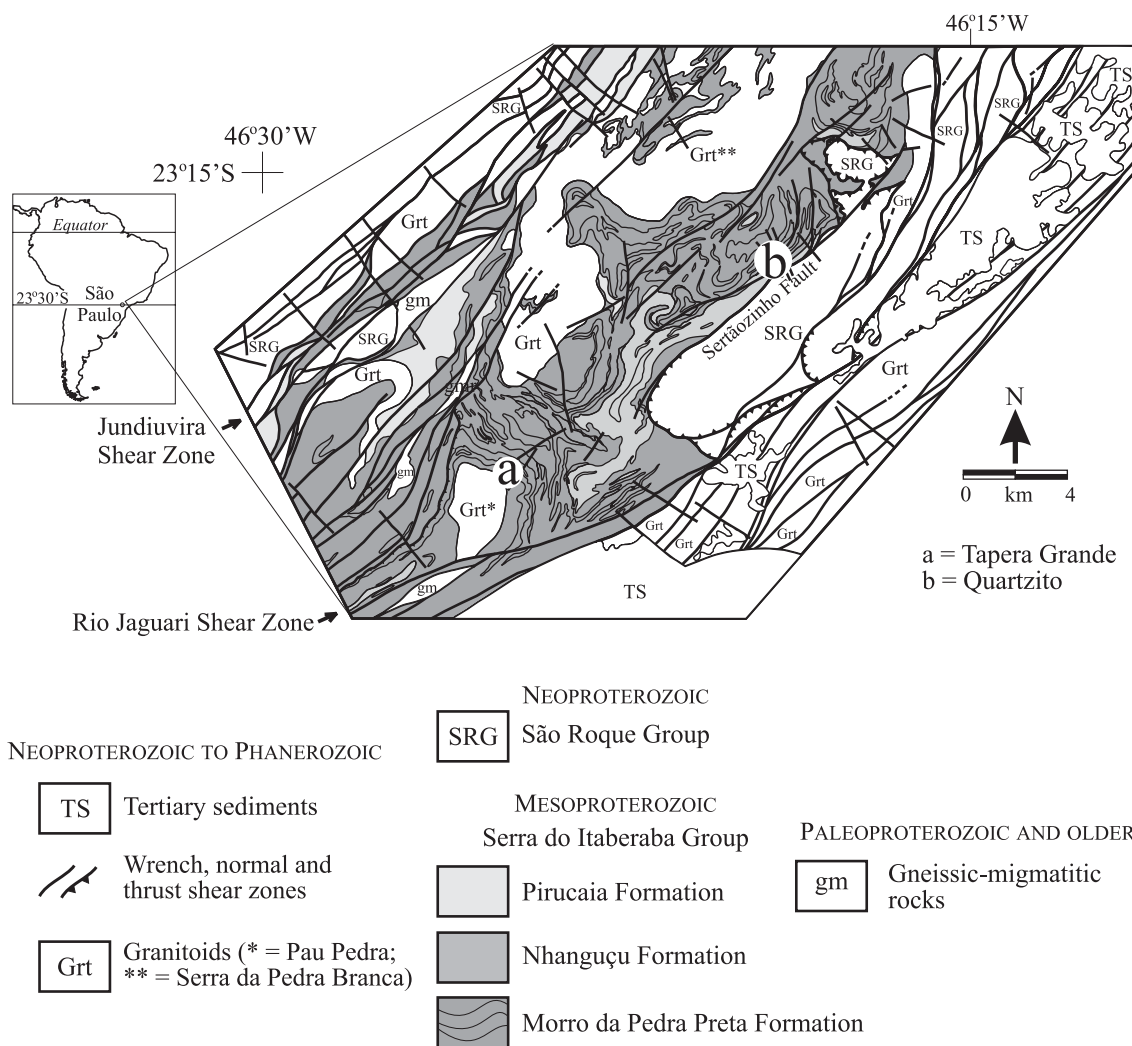


Fig. 1 – Simplified map of Serra do Itaberaba and São Roque Groups (modified from Juliani 1993).

and (meta)volcaniclastic rocks and tourmalinites) followed the closing of the Morro da Pedra Preta basin. On top of the Nhanguçu sequence fine-grained sediments were deposited in progressively shallower waters, and were affected by less intense exhalative volcanic activity.

The Pirucaia Formation (quartzites and quartz schists), possibly coeval with the Nhanguçu Formation, represents continental platform clastic sedimentation that took place in marginal parts of the Serra do Itaberaba basin.

The Serra do Itaberaba Group was metamorphosed to medium amphibolite facies, with the crystallization of kyanite, with later transformation to sillimanite. A second metamorphic event, most likely related to the Brasiliano Cycle, took place in the area, this time reaching the greenschist facies.

Deformed tonalitic and granodioritic granitoids in the region represent in part reworked portions of basement rocks, whereas porphyritic granite and granodiorite bodies, such

as the Pau Pedra pluton, intruded the Serra do Itaberaba Group in the Neoproterozoic (Brasiliano orogeny). These may be an extension of the nearby syn- to late-orogenic, calc-alkaline, 625 Ma-old Cantareira granitoid occurrence described by Janasi and Ulbrich (1991).

Shear zones such as Rio Jaguari and Jundiuvira and associated faults (e.g. Sertãozinho fault) were developed during transcurrent events that also affected the granitoid rocks.

TOURMALINES OF THE MORRO DA PEDRA PRETA FORMATION

A series of 25 drill cores were obtained from two areas informally named Tapera Grande (NE of the Pau Pedra granitoid body) and Quartzito (W of the Sertãozinho Fault), which sampled large part of the volcano-sedimentary sequence of the Morro da Pedra Preta Formation.

In both study areas (Fig. 1), tourmalines are found in the iron formation (including metachert and tourmalinites), psammites, calc-silicate rocks, basic metatuffs, metavolcaniclastic rocks, amphibolites, and quartz veins.

The iron formation is composed of quartz (50 to 75%), magnetite, hematite, iron oxides-hydroxides, and variable amounts of tourmaline. In this work, metachert and tourmalinites are considered sub-facies of the iron formation, according to the relative amounts of quartz (which may reach 100% in metachert) and tourmaline. In the metachert, very dark-colored, zoned, strongly pleochroic (from dark bluish green to light brown) tourmalines occur in an outcrop (sample LJ10A, Fig. 2A) close to SRT-1 drill hole. They form clusters or are aligned according to the general banding of the rock. Subordinately, chlorite also occurs in the metachert, as well as limonite and iron hydroxides.

Tourmaline-rich layers gradually turn into tourmalinites, as described by Slack (1982) and Plimer (1987, 1988). They appear as discontinuous, centimeter- to meter-thick lenses composed of alternating tourmaline-rich and quartz-rich bands. Such rocks are fine-grained and contain variable amounts of garnet, hornblende and sericite (after plagioclase). Features like rip-up clasts such as those described by Slack et al. (1984) in the Black Prince mine in Broken Hill (Australia), and Bone (1988) in the Rum Jungle area (Australia) also appear in the Morro da Pedra Preta Formation. The syn-sedimentary nature of the tourmalinites is attested by the S_1 foliation, which is marked by the tourmalines and is parallel to bedding. Tourmalinite lenses are sometimes folded, and tourmaline partially recrystallizes in S_2 , indicating a pre-metamorphic lamination affected by subsequent deformation (Juliani 1993).

Bluish green, strongly pleochroic tourmalines are found in 15 m thick, folded sequences of biotite to phlogopite quartz schists containing variable amounts of staurolite and garnet. Psammites grade into tourmaline-bearing calc-silicate rocks.

In the basic metatuffs (quartz hornblende schists) brownish green tourmalines appear together with garnet, biotite, chlorite, zoisite, apatite, and carbonate, either as lenses or disseminated in the matrix. They have a more well-developed schistosity that can be marked by opaque minerals. A tourmaline-bearing epidote, considered as resulting from the hydrothermal alteration (carbonatization) of basic metatuffs, occurs at depths of 84 m in the SRT-1 borehole.

The metavolcaniclastic rocks, which are very similar in composition to the basic metatuffs, contain titanomagnetites altering into ti-

tanite, abundant plagioclase, quartz, hornblende altering into biotite and chlorite, zoisite, and minor carbonate, apatite, and zircon. Garnet appears in variable amounts, mingled with hornblende. Tourmalines can be as abundant as hornblende. Tourmaline grains present dark, bluish cores and brown rims, and are slightly deformed.

The amphibolites are coarser-grained rocks formed by a felty mass of hornblende, containing biotite, interstitial quartz, and tourmaline that intergrows with amphibole, has dark, bluish cores and brown rims; occasionally it is associated with opaque minerals.

In general associated with shearing, quartz veins crosscut the whole Morro da Pedra Preta sequence. Tourmalines tend to occur concentrated in the contact between veins and country rock (Fig. 2B), associated with sulfides (pyrite and chalcopyrite) of sulfidation stages II, III and IV described by Beljanskis et al. (1999a).

In all rock types, tourmaline is usually fine-grained and presents basal sections from 1 to 5 mm in diameter, except when found arranged in comb texture in tourmaline-rich levels in the metachert, and in this case crystals are larger than 5 mm.

MATERIALS AND METHODS

The samples chosen for analyses (scanning electron microscopy, Raman spectrometry, X-ray diffraction fluorescence, and oxygen and hydrogen isotopic analysis) were collected from tourmalinite (outcrop T12 – Tapera Grande), tourmaline-rich metachert (outcrops LF10, LJ09, and LJ10 – Tapera Grande; drill hole F01-1B at 3.80m depth – Quartzito), and quartz veins (drill holes SRT3-99 at 54.10m depth – Tapera Grande; FQ-112-3a and FQ-112-3b at 18.40m depth, and FQ-112-46-3 at

46.23 m depth – Quartzito).

For scanning electron microscopy and Raman spectrometry, polished thin sections of the rock samples were prepared at the Petrology and Rock Technology Laboratory of the Technological Research Institute of São Paulo State (IPT).

Energy dispersive X-ray microanalyses (EDS-SEM) of carbon-coated polished thin sections were carried out at the Scanning Electron Microscope Laboratory of the Geosciences Institute of the Campinas State University (IGe-UNICAMP), equipped with a LEO scanning electron microscope model 430 I. The conditions adopted during analyses were: interaction time = 100 seconds; accelerating voltage = 20 kV.

Raman analyses were also carried out at IGe-UNICAMP. The equipment is a laser-Raman multi-channel microprobe (CCD T64000 JOBIN-YVON) coupled with a high-resolution optical microscope (OLYMPUS-BHS) that focuses the laser radiation (Ar laser, line 514.5 nm, 80 mW) on the sample (1 μ m-diameter aperture). A Sony video system helps monitor the laser operation. Beam-sample interaction time adopted was 300 s. The Raman frequencies were calibrated to 1cm⁻¹ using standard Ne emission lines.

For X-ray diffraction fluorescence, and oxygen and hydrogen stable isotope studies, quartz and tourmaline separates were obtained at the Sample Preparation Laboratory of the Geosciences Institute of São Paulo University – IGe-USP. Crushing of rock chips and screening were followed by heavy liquid separation of quartz and tourmaline, Franz electromagnetic separation of impurities, and hand picking under a binocular microscope.

X-ray diffraction fluorescence analyses

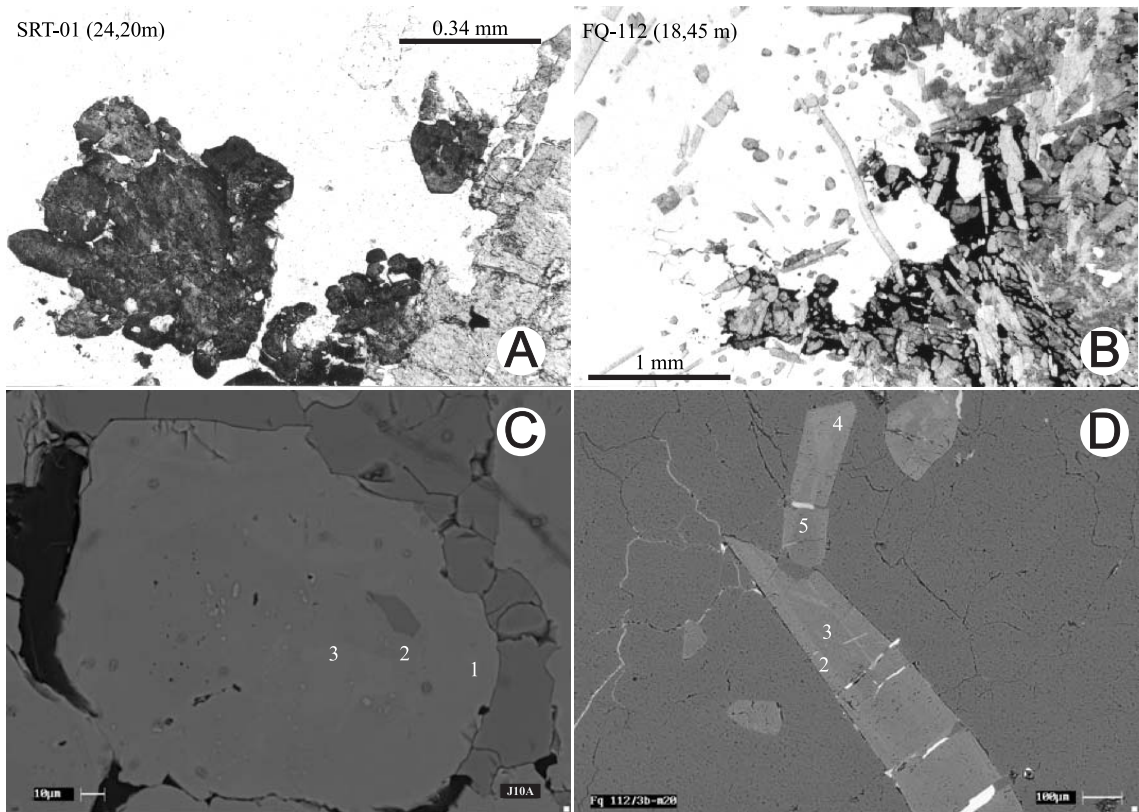


Fig. 2 – B&W photomicrographs of A: very dark, zoned, strongly pleochroic tourmalines from Tapera Grande metachert (plane-polarized light), and B: zoned tourmaline needles of Quartzito quartz vein (plane-polarized light). SEM images of C: zoned tourmaline crystal from Tapera Grande metachert (to points 1, 2 and 3 correspond analyses 19, 20 and 21 in Table I), and D: zoned tourmaline needles of Quartzito quartz vein, also shown in B (to point 2 correspond analyses 63 and 64; to point 3, analyses 67, 68 and 71; to point 4, analyses 72, 75 and 76, and point 5, analyses 79 and 80 in Table I).

took place at the XRF Laboratory of IGc-USP. Oxygen and hydrogen stable isotope analyses were carried out at the Scottish Universities Environmental Research Center (East Kilbride, UK), the former with the laser fluorination method (Fallick et al. 1992) and the latter by the conventional method of gas extraction.

RESULTS

EDS-SEM MINERAL ANALYSES

Table I presents tourmaline compositions obtained by EDS-SEM, with total weight % of oxides normalized to 100%. Analyses 1 to 21

(Tapera Grande), and 40 and 41 (Quartzito) correspond to tourmalines from metachert; analyses 22 to 30 correspond to tourmalines from a tourmalinite from Tapera Grande (T12); analyses 36 to 39 to tourmalines from a quartz vein from Tapera Grande (SRT3-99), and 44 to 85 to tourmalines from quartz veins of Quartzito (112/3a, 112/3b and 112/46-3).

The structural formulae were calculated according to Henry and Guidotti (1985), assuming 3 boron and 31 oxygen atoms per formula unit (apfu).

Calculations were made using Microsoft

TABLE I

EDS-SEM analyses of tourmalines from Tapera Grande and Quartzito.
Structural formulae calculated on 31 oxygen basis.

Sample	T a p e r a G r a n d e							
	LF10 1	LF10 2	LF10 3	LF10 4	LF-10b 5	LF-10b 6	LF10 11	LJ09 15
SiO ₂	42.97	42.90	41.10	41.61	40.41	39.55	37.58	38.48
TiO ₂	0.58	0.62	0.00	0.00	0.22	0.68	0.19	0.68
Al ₂ O ₃	34.01	35.10	36.71	36.59	37.62	37.87	36.94	35.81
FeO	13.26	13.56	12.15	12.14	12.92	11.47	16.07	14.44
MgO	5.74	4.80	5.39	5.26	5.45	6.09	4.73	6.17
CaO	1.11	0.60	0.45	0.59	0.49	0.92	0.47	1.01
Na ₂ O	2.34	2.42	4.19	3.81	2.89	3.43	4.02	3.41
B	3.000	3.000	3.000	3.000	3.000	3.000	3.000	3.000
Al _{total}	5.777	5.954	6.243	6.209	6.394	6.432	6.440	6.195
Si _{total}	6.191	6.172	5.927	5.989	5.826	5.698	5.558	5.646
Si _T	6.000	6.000	5.927	5.989	5.826	5.698	5.558	5.646
Al _T	0.000	0.000	0.073	0.011	0.174	0.302	0.442	0.354
Al _Z	5.777	5.954	6.000	6.000	6.000	6.000	5.998	5.841
Fe ³⁺	0.223	0.046	0.000	0.000	0.000	0.000	0.002	0.159
Al _Y	0.000	0.000	0.170	0.197	0.219	0.130	0.000	0.000
Si _Y	0.191	0.172	0.000	0.000	0.000	0.000	0.000	0.000
Ti	0.063	0.067	0.000	0.000	0.024	0.073	0.021	0.075
Fe _{total}	1.598	1.631	1.465	1.461	1.558	1.382	1.988	1.772
Fe ²⁺	1.376	1.586	1.465	1.461	1.558	1.382	1.986	1.614
Mg	1.231	1.029	1.160	1.127	1.172	1.308	1.044	1.349
Y _{total}	2.861	2.854	2.795	2.786	2.973	2.893	3.050	3.037
Ca	0.171	0.092	0.070	0.091	0.076	0.142	0.075	0.159
Na	0.653	0.676	1.172	1.062	0.807	0.957	1.152	0.971
X _{total}	0.824	0.768	1.242	1.152	0.883	1.099	1.228	1.130
[]	0.176	0.232	-0.242	-0.152	0.117	-0.099	-0.228	-0.130
Total	15.684	15.622	16.037	15.938	15.857	15.991	16.278	16.167
R1	0.824	0.768	1.242	1.152	0.883	1.099	1.228	1.130
R2	2.607	2.615	2.625	2.589	2.730	2.690	3.029	2.962
R1+R2	3.431	3.383	3.867	3.741	3.613	3.788	4.257	4.093
R3	5.861	6.044	6.243	6.209	6.426	6.529	6.468	6.295
Mg#	0.435	0.387	0.442	0.436	0.429	0.486	0.344	0.432

TABLE I (continuation)

Sample	T a p e r a			G r a n d e				
	LJ09 16	LJ09 17	LJ09 18	LJ10A 19	LJ10A 20	LJ10A 21	T12 22	T12 23
SiO ₂	39.72	41.58	43.31	39.50	39.89	39.19	40.28	45.07
TiO ₂	0.83	1.12	0.25	1.00	0.32	0.51	0.93	0.19
Al ₂ O ₃	36.60	32.09	35.46	36.13	37.26	34.51	38.21	36.58
FeO	13.23	17.49	13.04	14.41	12.84	17.07	15.19	8.13
MgO	5.93	4.46	5.15	5.29	6.16	4.81	2.81	7.36
CaO	0.89	1.41	0.52	0.96	0.85	1.02	0.78	0.41
Na ₂ O	2.80	1.85	2.27	2.71	2.67	2.89	1.81	2.26
B	3.000	3.000	3.000	3.000	3.000	3.000	3.000	3.000
Al _{total}	6.256	5.578	5.989	6.212	6.347	6.022	6.530	6.020
Si _{total}	5.759	6.130	6.204	5.761	5.763	5.801	5.839	6.291
Si _T	5.759	6.000	6.000	5.761	5.763	5.801	5.839	6.000
Al _T	0.241	0.000	0.000	0.239	0.237	0.199	0.161	0.000
Al _Z	6.000	5.578	5.989	5.973	6.000	5.823	6.000	6.000
Fe ³⁺	0.000	0.422	0.011	0.027	0.000	0.177	0.000	0.000
Al _Y	0.015	0.000	0.000	0.000	0.110	0.000	0.369	0.020
Si _Y	0.000	0.130	0.204	0.000	0.000	0.000	0.000	0.291
Ti	0.090	0.125	0.027	0.110	0.035	0.057	0.102	0.020
Fe _{total}	1.604	2.157	1.563	1.757	1.551	2.114	1.842	0.949
Fe ²⁺	1.604	1.735	1.551	1.731	1.551	1.937	1.842	0.949
Mg	1.281	0.979	1.099	1.149	1.326	1.061	0.606	1.531
Y _{total}	2.991	2.969	2.881	2.990	3.022	3.054	2.919	2.812
Ca	0.138	0.222	0.080	0.150	0.132	0.162	0.121	0.061
Na	0.787	0.529	0.630	0.766	0.749	0.829	0.509	0.613
X _{total}	0.925	0.751	0.710	0.916	0.881	0.991	0.629	0.673
[]	0.075	0.249	0.290	0.084	0.119	0.009	0.371	0.327
Total	15.916	15.721	15.590	15.906	15.903	16.045	15.549	15.485
R1	0.925	0.751	0.710	0.916	0.881	0.991	0.629	0.673
R2	2.886	2.714	2.650	2.880	2.877	2.997	2.448	2.480
R1+R2	3.811	3.466	3.360	3.796	3.758	3.988	3.078	3.154
R3	6.376	5.744	6.024	6.359	6.393	6.098	6.666	6.047
Mg#	0.444	0.312	0.413	0.395	0.461	0.334	0.248	0.617

TABLE I (continuation)

Sample	T a p e r a				G r a n d e			
	T12 24	T12 25	T12a 27	T12a 28	T12a 29	T12a 30	SRT3-99 36	SRT3-99 37
SiO ₂	44.48	44.38	42.07	40.74	40.73	43.26	41.35	42.48
TiO ₂	0.82	0.37	0.68	1.02	1.13	0.73	1.05	0.86
Al ₂ O ₃	35.44	36.47	36.39	36.06	36.17	36.81	31.54	34.89
FeO	10.28	10.70	13.27	15.11	15.89	10.48	18.11	11.93
MgO	6.36	5.69	5.68	4.29	3.46	5.49	4.64	5.89
CaO	0.47	0.39	0.00	0.66	0.50	0.38	1.27	1.08
Na ₂ O	2.16	1.99	1.91	2.13	2.12	2.86	2.04	2.86
B	3.000	3.000	3.000	3.000	3.000	3.000	3.000	3.000
Al _{total}	5.899	6.068	6.150	6.178	6.212	6.151	5.507	5.906
Si _{total}	6.280	6.264	6.029	5.921	5.935	6.133	6.123	6.099
Si _T	6.000	6.000	6.000	5.921	5.935	6.000	6.000	6.000
Al _T	0.000	0.000	0.000	0.079	0.065	0.000	0.000	0.000
Al _Z	5.899	6.000	6.000	6.000	6.000	6.000	5.507	5.906
Fe ³⁺	0.101	0.000	0.000	0.000	0.000	0.000	0.493	0.094
Al _Y	0.000	0.068	0.150	0.100	0.147	0.151	0.000	0.000
Si _Y	0.280	0.264	0.029	0.000	0.000	0.133	0.123	0.099
Ti	0.087	0.040	0.074	0.111	0.123	0.077	0.117	0.093
Fe _{total}	1.214	1.263	1.590	1.837	1.936	1.242	2.242	1.432
Fe ²⁺	1.113	1.263	1.590	1.837	1.936	1.242	1.749	1.338
Mg	1.337	1.197	1.214	0.928	0.752	1.160	1.024	1.260
Y _{total}	2.818	2.831	3.056	2.976	2.958	2.764	3.013	2.790
Ca	0.070	0.059	0.000	0.103	0.078	0.057	0.201	0.167
Na	0.590	0.544	0.531	0.600	0.600	0.786	0.585	0.797
X _{total}	0.661	0.604	0.531	0.703	0.678	0.843	0.786	0.964
[]	0.339	0.396	0.469	0.297	0.322	0.157	0.214	0.036
Total	15.478	15.435	15.588	15.679	15.636	15.607	15.799	15.754
R1	0.661	0.604	0.531	0.703	0.678	0.843	0.786	0.964
R2	2.451	2.460	2.804	2.765	2.688	2.402	2.773	2.598
R1+R2	3.111	3.064	3.335	3.468	3.366	3.245	3.559	3.562
R3	6.015	6.120	6.248	6.326	6.376	6.254	5.662	6.029
Mg#	0.524	0.487	0.433	0.336	0.280	0.483	0.313	0.468

TABLE I (continuation)

T a p e r a G r a n d e			Q u a r t z i t o			
Sample	SRT-3-99	SRT-3-99	F01-1B	F01-1B	112/3a-m10	112/3a-m10
	38	39	40	41	44	47
SiO ₂	38.38	39.40	40.05	39.63	41.29	41.36
TiO ₂	1.11	0.72	0.76	0.00	0.69	0.69
Al ₂ O ₃	34.84	35.45	37.52	39.48	37.48	37.51
FeO	16.98	15.37	11.86	13.25	9.08	8.94
MgO	5.34	5.32	5.55	3.75	9.66	9.60
CaO	1.17	1.08	0.90	0.51	1.80	1.90
Na ₂ O	2.17	2.67	3.37	3.38	< d.l.	< d.l.
Cr ₂ O ₃	n.d.	n.d.	n.d.	n.d.	< d.l.	< d.l.
B	3.000	3.000	3.000	3.000	3.000	3.000
Al _{total}	6.078	6.128	6.375	6.724	6.228	6.230
Si _{total}	5.679	5.777	5.772	5.726	5.820	5.827
Si _T	5.679	5.777	5.772	5.726	5.820	5.827
Al _T	0.321	0.223	0.228	0.274	0.180	0.173
Al _Z	5.757	5.905	6.000	6.000	6.000	6.000
Fe ³⁺	0.243	0.095	0.000	0.000	0.000	0.000
Al _Y	0.000	0.000	0.147	0.450	0.048	0.056
Si _Y	0.000	0.000	0.000	0.000	0.000	0.000
Ti	0.124	0.079	0.082	0.000	0.073	0.073
Fe _{total}	2.101	1.884	1.429	1.601	1.070	1.053
Fe ²⁺	1.858	1.789	1.429	1.601	1.070	1.053
Mg	1.178	1.162	1.192	0.808	2.030	2.016
Cr	–	–	–	–	–	–
Y _{total}	3.160	3.030	2.850	2.859	3.221	3.198
Ca	0.186	0.170	0.139	0.079	0.272	0.288
Na	0.624	0.760	0.941	0.947	0.000	0.000
X _{total}	0.810	0.930	1.079	1.026	0.272	0.288
[]	0.190	0.070	–0.079	–0.026	0.728	0.712
Total	15.970	15.960	15.929	15.885	15.493	15.486
R1	0.810	0.930	1.079	1.026	0.272	0.288
R2	3.036	2.951	2.621	2.409	3.100	3.069
R1+R2	3.846	3.881	3.700	3.435	3.372	3.356
R3	6.243	6.233	6.484	6.724	6.325	6.326
Mg#	0.359	0.381	0.455	0.335	0.655	0.657

n.d. = not determined; < d.l. = below detection limit.

TABLE I (continuation)

Q u a r t z i t o						
Sample	112/3a-m10 48	112/3a-m10 51	112/3a-m10 52	112/3a-m10 53	112/3a-m10 56	112/3b-m20 63
SiO ₂	41.25	42.33	42.21	41.50	42.02	41.34
TiO ₂	0.95	0.00	0.23	0.57	0.31	0.57
Al ₂ O ₃	36.26	38.88	38.82	37.90	38.88	38.52
FeO	10.29	8.98	8.94	8.48	8.74	8.84
MgO	9.11	8.83	8.83	9.78	9.08	8.92
CaO	2.13	0.97	0.97	1.78	0.97	1.45
Na ₂ O	< d.l.					
Cr ₂ O ₃	< d.l.	0.36				
B	3.000	3.000	3.000	3.000	3.000	3.000
Al _{total}	6.071	6.413	6.405	6.275	6.413	6.382
Si _{total}	5.858	5.922	5.906	5.828	5.878	5.810
Si _T	5.858	5.922	5.906	5.828	5.878	5.810
Al _T	0.142	0.078	0.094	0.172	0.122	0.190
Al _Z	5.929	6.000	6.000	6.000	6.000	6.000
Fe ³⁺	0.071	0.000	0.000	0.000	0.000	0.000
Al _Y	0.000	0.335	0.310	0.103	0.290	0.192
Si _Y	0.000	0.000	0.000	0.000	0.000	0.000
Ti	0.101	0.000	0.024	0.061	0.032	0.061
Fe _{total}	1.222	1.050	1.046	0.996	1.022	1.039
Fe ²⁺	1.151	1.050	1.046	0.996	1.022	1.039
Mg	1.928	1.841	1.841	2.047	1.894	1.867
Cr	–	–	–	–	–	0.040
Y _{total}	3.180	3.226	3.222	3.207	3.238	3.200
Ca	0.325	0.145	0.145	0.267	0.145	0.218
Na	0.000	0.000	0.000	0.000	0.000	0.000
X _{total}	0.325	0.145	0.145	0.267	0.145	0.218
[]	0.675	0.855	0.855	0.733	0.855	0.782
Total	15.505	15.372	15.368	15.474	15.384	15.418
R1	0.325	0.145	0.145	0.267	0.145	0.218
R2	3.079	2.892	2.888	3.043	2.916	2.907
R1+R2	3.403	3.037	3.033	3.310	3.061	3.125
R3	6.206	6.413	6.437	6.356	6.456	6.463
Mg#	0.612	0.637	0.638	0.673	0.650	0.642

n.d. = not determined; < d.l. = below detection limit.

TABLE I (continuation)

Q u a r t z i t o						
Sample	112/3b-m20 64	112/3b-m20 67	112/3b-m20 68	112/3b-m20 71	112/3b-m20 72	112/3b-m20 75
SiO ₂	41.35	42.07	41.93	41.73	41.84	41.82
TiO ₂	0.38	0.27	0.35	0.27	0.27	0.38
Al ₂ O ₃	38.92	39.37	38.39	39.18	39.55	38.89
FeO	8.81	8.12	8.38	8.22	8.37	8.48
MgO	8.81	8.82	9.45	9.09	8.81	8.98
CaO	1.40	1.11	1.32	1.19	1.16	1.18
Na ₂ O	< d.l.					
Cr ₂ O ₃	0.33	0.26	0.18	0.33	0.00	0.26
V ₂ O ₅	< d.l.					
B	3.000	3.000	3.000	3.000	3.000	3.000
Al _{total}	6.443	6.477	6.337	6.458	6.513	6.417
Si _{total}	5.806	5.870	5.870	5.835	5.845	5.854
Si _T	5.806	5.870	5.870	5.835	5.845	5.854
Al _T	0.194	0.130	0.130	0.165	0.155	0.146
Al _Z	6.000	6.000	6.000	6.000	6.000	6.000
Fe ³⁺	0.000	0.000	0.000	0.000	0.000	0.000
Al _Y	0.249	0.346	0.207	0.293	0.358	0.271
Si _Y	0.000	0.000	0.000	0.000	0.000	0.000
Ti	0.040	0.028	0.036	0.028	0.028	0.040
Fe _{total}	1.035	0.947	0.982	0.961	0.978	0.993
Fe ²⁺	1.035	0.947	0.982	0.961	0.978	0.993
Mg	1.843	1.834	1.971	1.893	1.833	1.873
Cr	0.036	0.028	0.020	0.036	0.000	0.028
V	–	–	–	–	–	–
Y _{total}	3.204	3.184	3.217	3.212	3.197	3.205
Ca	0.210	0.165	0.198	0.178	0.174	0.178
Na	0.000	0.000	0.000	0.000	0.000	0.000
X _{total}	0.210	0.165	0.198	0.178	0.174	0.178
[]	0.790	0.835	0.802	0.822	0.826	0.822
Total	15.414	15.349	15.415	15.390	15.370	15.383
R1	0.210	0.165	0.198	0.178	0.174	0.178
R2	2.878	2.781	2.953	2.854	2.811	2.866
R1+R2	3.088	2.947	3.151	3.032	2.984	3.044
R3	6.496	6.514	6.385	6.496	6.551	6.471
Mg#	0.640	0.659	0.668	0.663	0.652	0.653

n.d. = not determined; < d.l. = below detection limit.

TABLE I (continuation)

Q u a r t z i t o					
Sample	112/3b-m20 76	112/3b-m20 79	112/3b-m20 80	112/46-3 84	112/46-3 85
SiO ₂	41.89	42.60	42.43	41.78	41.27
TiO ₂	0.35	0.00	0.00	0.00	0.00
Al ₂ O ₃	39.21	39.02	38.87	39.18	39.53
FeO	8.42	8.04	8.10	7.10	7.09
MgO	8.69	9.60	9.58	10.13	10.33
CaO	1.27	0.73	0.76	1.81	1.77
Na ₂ O	< d.l.	< d.l.	< d.l.	< d.l.	< d.l.
Cr ₂ O ₃	0.18	< d.l.	< d.l.	< d.l.	< d.l.
V ₂ O ₅	< d.l.	< d.l.	0.26	< d.l.	< d.l.
B	3.000	3.000	3.000	3.000	3.000
Al _{total}	6.465	6.403	6.383	6.437	6.499
Si _{total}	5.858	5.929	5.910	5.822	5.756
Si _T	5.858	5.929	5.910	5.822	5.756
Al _T	0.142	0.071	0.090	0.178	0.244
Al _Z	6.000	6.000	6.000	6.000	6.000
Fe ³⁺	0.000	0.000	0.000	0.000	0.000
Al _Y	0.322	0.332	0.293	0.259	0.255
Si _Y	0.000	0.000	0.000	0.000	0.000
Ti	0.036	0.000	0.000	0.000	0.000
Fe _{total}	0.984	0.936	0.944	0.828	0.827
Fe ²⁺	0.984	0.936	0.944	0.828	0.827
Mg	1.811	1.992	1.988	2.103	2.147
Cr	0.020	–	–	–	–
V	–	–	0.024	–	–
Y _{total}	3.174	3.260	3.249	3.189	3.229
Ca	0.190	0.109	0.113	0.271	0.265
Na	0.000	0.000	0.000	0.000	0.000
X _{total}	0.190	0.109	0.113	0.271	0.265
[]	0.810	0.891	0.887	0.729	0.735
Total	15.364	15.369	15.362	15.460	15.494
R1	0.190	0.109	0.113	0.271	0.265
R2	2.795	2.928	2.932	2.930	2.974
R1+R2	2.985	3.037	3.045	3.201	3.239
R3	6.513	6.403	6.383	6.437	6.499
Mg#	0.648	0.680	0.678	0.718	0.722

n.d. = not determined; < d.l. = below detection limit.

Excel worksheets and checked with Yavuz's (1997) TOURMAL program, that assumes for Fe^{3+} calculation full occupancy of T and Z sites:

$$T = \text{Si} + \text{Al}^{\text{IV}} = 6.000$$

$$Z = \text{Al}^{\text{IV}} + \text{Fe}^{3+} = 6.000$$

Yavuz (1997) calculates the R1, R2 and R3 parameters as follows:

$$R1 = \text{Na} + \text{Ca}$$

$$R2 = \text{Fe}_{\text{total}} + \text{Mg}$$

$$R3 = \text{Al} + 1.33 \text{ Ti}$$

Tourmaline compositions are represented in Figure 3, which is a Henry and Guidotti's (1985) Al- Fe_{tot} -Mg diagram (molecular proportions). Tourmalines from metachert of Tapera Grande and Quartzito, and quartz veins of Tapera Grande fall on the line limiting field 2 (*Li-poor granitoids and their associated pegmatites and aplites*), field 4 (*metapelites and metapsammites coexisting with an Al-saturating phase*) and field 5 (*metapelites and metapsammites not coexisting with an Al-saturating phase*), corresponding to intermediate schorl-dravite. Tourmalines of quartz veins from Quartzito fall in field 5.

In the Ca- Fe_{tot} -Mg diagram (Fig. 4), tourmalines from metachert of Tapera Grande and Quartzito, tourmalinite and quartz veins of Tapera Grande fall in field 2 (*Li-poor granitoids and their associated pegmatites and aplites*) and 4 (*Ca-poor metapelites, metapsammites, and quartz-tourmaline rocks*), whereas tourmalines from quartz veins of Quartzito fall in field 4.

Differently from the other tourmalines, those from tourmalinite T12 show large $\text{Al}_{50}\text{Fe}(\text{total})_{50}$ and $\text{Al}_{50}\text{Mg}_{50}$ variation. These compositions are similar to those presented by Plimer (1988), which describes tourmalines from tourmalinites of eight different localities

in Australia. The triangular diagrams also show that T12 tourmaline compositions are intermediate between those obtained for metachert and Quartzito quartz veins. Tourmaline compositions corresponding to Quartzito quartz veins match those found in Plimer (1986), Bone (1988), and King and Kerrich (1989).

Triangular diagrams of Figs. 3 and 4 show that Mg is a good discriminant factor that distinguishes Tapera Grande tourmalines from those of Quartzito quartz veins, i.e. the latter are Mg-richer than the former.

It is worth mentioning that even when K_2O (in all analyses) and Na_2O (in tourmalines of Quartzito quartz veins) contents are below detection limits of EDS-SEM, yielding incomplete structural formulae, positive correlation between Mg# [= $\text{Mg}/(\text{Mg} + \text{Fe}_{\text{total}})$] and X-site vacancy ($\square_{\text{X}} = 1 - \text{Ca} - \text{Na} - \text{K}$) is obtained, as depicted from Table I:

Metachert:

$$\text{Mg\#} = 0.31-0.49; \quad \square_{\text{X}} = 0-0.24$$

Tapera Grande quartz veins:

$$\text{Mg\#} = 0.31-0.47; \quad \square_{\text{X}} = 0.04-0.21$$

Tourmalinite:

$$\text{Mg\#} = 0.25-0.62; \quad \square_{\text{X}} = 0.16-0.47$$

Quartzito quartz veins:

$$\text{Mg\#} = 0.61-0.68; \quad \square_{\text{X}} = 0.68-0.89$$

Tourmalines of Quartzito quartz veins stand out not only for their higher MgO contents, and NaO contents below EDS-SEM detection, but also for the presence of Cr and sometimes V. Once Na results null in the structural formula and Ca is very low (0.11-0.21), X-site vacancy reaches very high values (0.68-0.89). On the other hand, Mg can be as high as 1.81-1.99, causing $Y_{\text{total}} > 3$; exceeding Al results in Al_{T} from 0.07 to 0.19 (once $\text{Si} < 6$) and Al_{Y} from 0.19 to 0.36, accompanied by either

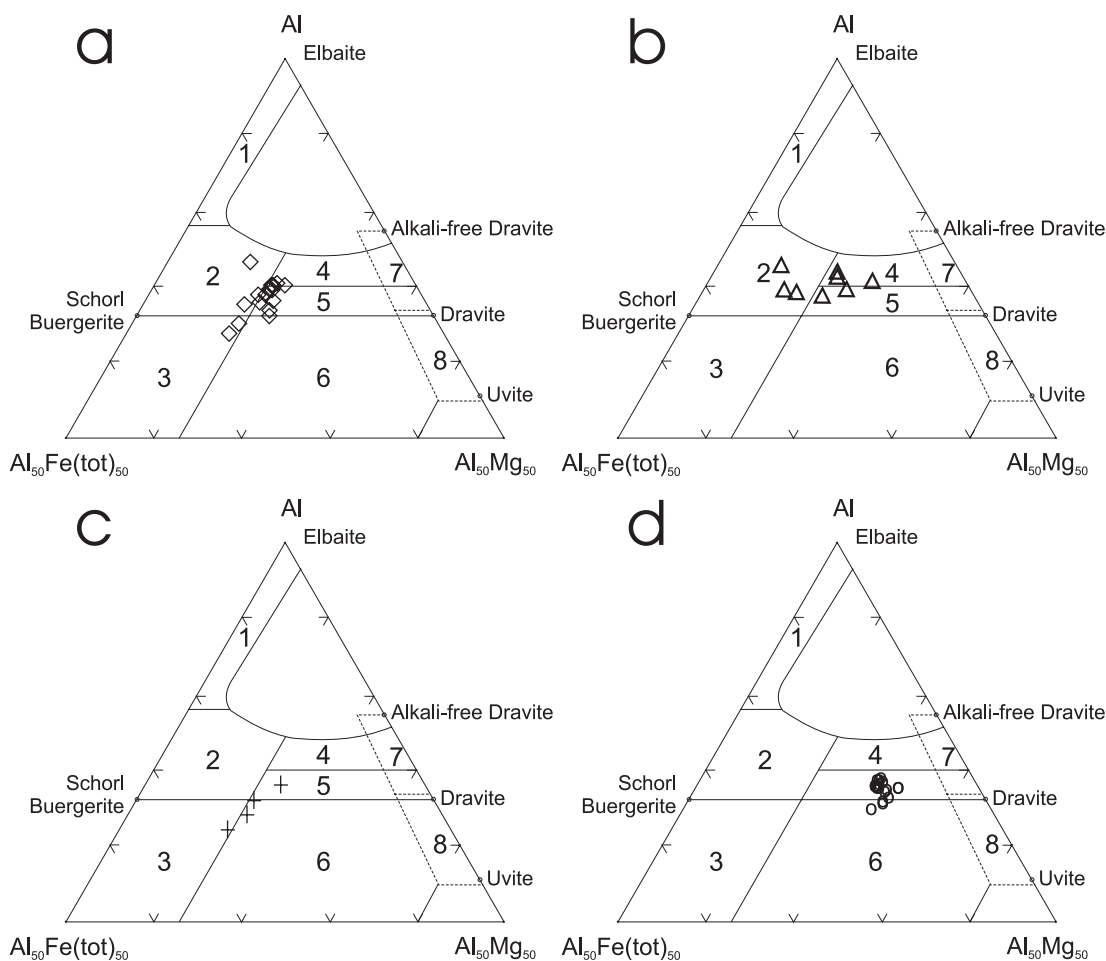


Fig. 3 – Representation of tourmaline compositions in Henry and Guidotti's (1985) Al-Fe_{tot}-Mg diagram (molecular proportions). Tourmalines from: (a) metachert – Tapera Grande and Quartzito; (b) tourmalinite – Tapera Grande; (c) quartz vein – Tapera Grande, and (d) quartz vein – Quartzito. Fields: (1) Li-rich granitoid pegmatites and aplites; (2) Li-poor granitoids and their associated pegmatites and aplites; (3) Fe³⁺ rich quartz-tourmaline rocks (hydrothermally altered granites); (4) metapelites and metapsammities coexisting with an Al-saturating phase; (5) metapelites and metapsammities not coexisting with an Al-saturating phase; (6) Fe³⁺ rich quartz-tourmaline rocks, calc-silicate rocks, and metapelites; (7) low-Ca metaultramafics and Cr, V-rich metasediments, and (8) metacarbonates and metapyroxenites.

Cr (0-0.04) or V (0-0.02).

R1+R2 vs. R3 diagrams (Fig. 5) show that tourmaline compositions from Quartzito quartz veins fall on the $\{\square\text{Al}\} \{\text{Na}[\text{Fe}, \text{Mg}]\}_{-1}$ vector, which represents the exchange schorl-dravite \rightarrow foitite.

Slightly zoned crystals also illustrate the general behavior of Tapera Grande and Quartz-

ito tourmaline compositions. Analyses 19, 20 and 21 in Table I correspond to points at rim, intermediate position and core of a LJ10A (metachert of Tapera Grande) tourmaline crystal (Fig. 2C). Numbers of Al and Mg apfu increase from point 1 to 2 and decrease to inner point 3, whereas Fe_{total} and Na apfu decrease from 1 to 2 followed by increase from 2 to 3

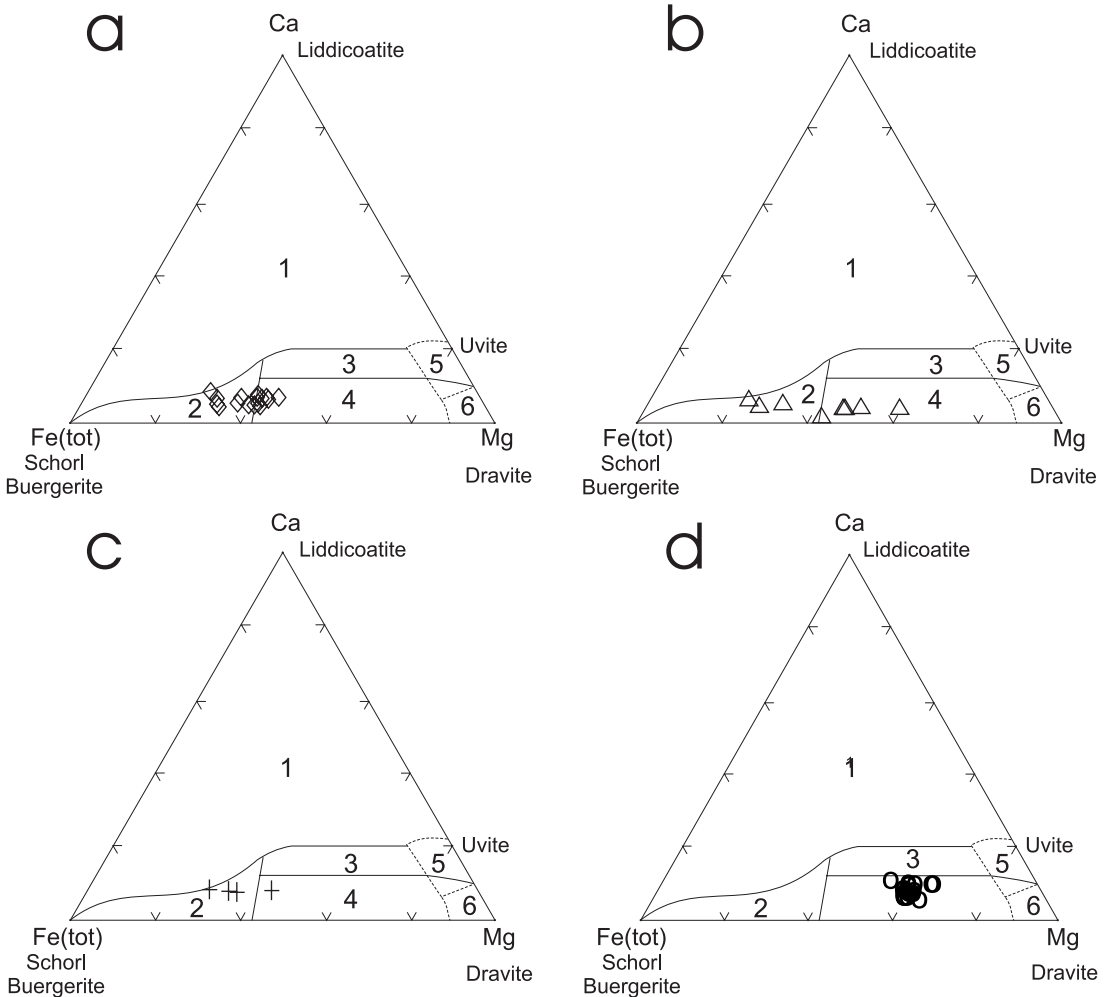


Fig. 4 – Representation of tourmaline compositions in Henry and Guidotti's (1985) Ca-Fe_{tot}-Mg diagram (molecular proportions). Tourmalines from: (a) metachert – Tapera Grande and Quartzito; (b) tourmalinite – Tapera Grande; (c) quartz vein – Tapera Grande, and (d) quartz vein – Quartzito. Fields: (1) Li-rich granitoid pegmatites and aplites; (2) Li-poor granitoids and their associated pegmatites and aplites; (3) Ca-rich metapelites, metapsammites, and calc-silicate rocks; (4) Ca-poor metapelites, metapsammites, and quartz-tourmaline rocks; (5) metacarbonates, and (6) metaultramafics.

(Fig. 6). The number of Fe_{total} apfu is higher than Mg.

Zoned crystals of T12 tourmaline (analyses 23, 24 and 25 in Table I) show discrete decreasing Mg and Na apfu, and increasing Fe_{total} apfu from rim to core (Fig. 6), and slight Al apfu decrease and Ti and Ca apfu increase in

an intermediate position between rim and core (analysis 24).

Figure 2D shows two zoned tourmaline needles of Quartzito quartz vein (FQ112-3b), which are also illustrated in Figure 2B, and the location of the points analyzed by EDS-SEM. Average values of analyses 63 and 64 (point 2,

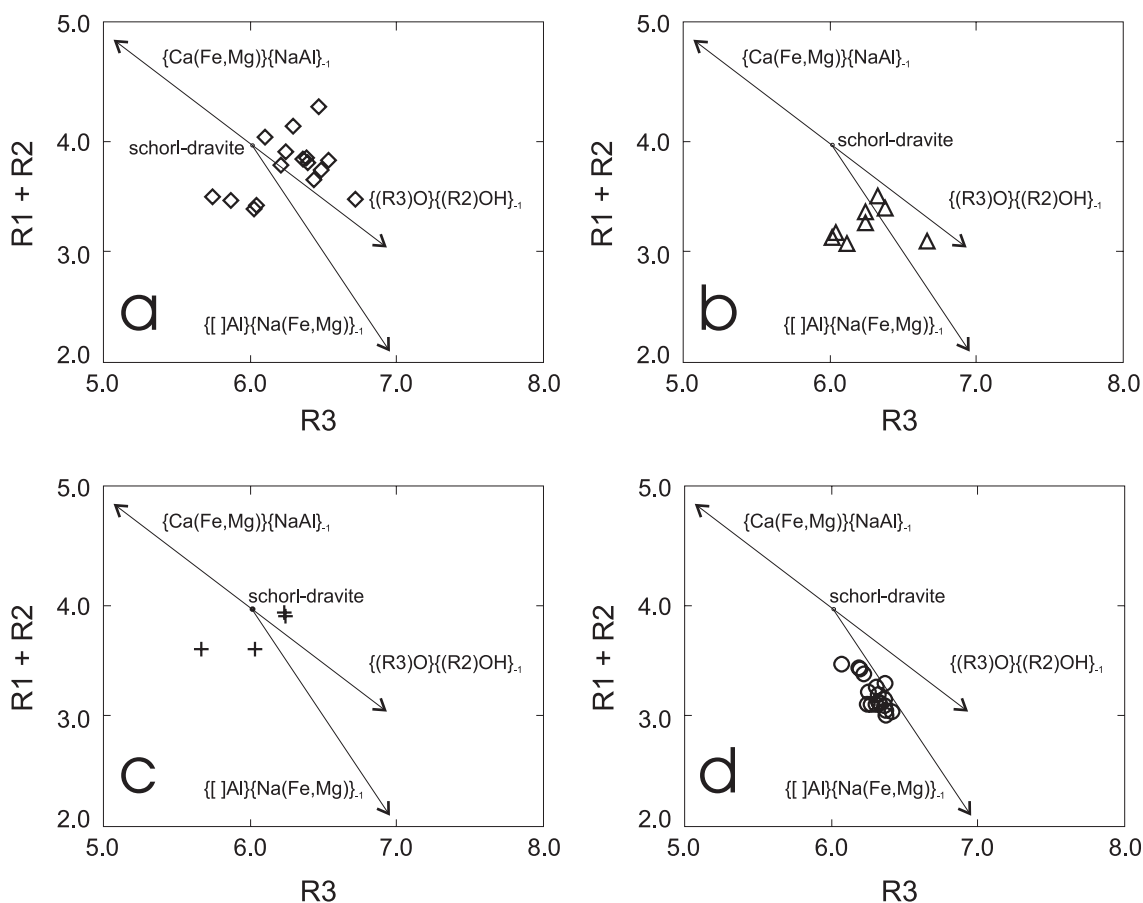


Fig. 5 – Representation of tourmaline compositions in the R1 + R2 vs. R3 diagram (R1, R2 and R3 calculated after Yavuz 1997). Tourmalines from: (a) metachert – Tapera Grande and Quartzito; (b) tourmalinite – Tapera Grande; (c) quartz vein – Tapera Grande, and (d) quartz vein – Quartzito.

at rim) and 67, 68 and 71 (point 3, at core) and analyses 72, 75 and 76 (point 4, at rim) and 79 and 80 (point 5, at core) are represented in Figure 6. The main compositional distinctions from rim to core are increase of Si and Mg apfu and decrease of Al and Fe_{total} apfu, and at the rims higher Ti, Fe and Ca apfu. Cr seems to be higher at rims than at cores (Table I).

X-RAY FLUORESCENCE ANALYSES OF MINERAL SEPARATES

As stated by Yavuz (1997), normalization based on 31 atoms of oxygen causes the exaggera-

tion of the relative importance of alkali-defect substitution. However, as previously stated, high X-site vacancies in tourmalines of Quartzito quartz veins resulted from NaO (and K_2O) contents below EDS-SEM detection limits, and relatively low CaO contents.

In order to check the actual X-site deficiency, tourmaline separates from tourmaline-bearing quartz veins of Tapera Grande (SRT2-97 and SRT3-99) and Quartzito (FQ112-3a) were analyzed by X-ray fluorescence. The analyses confirmed that the Quartzito samples are indeed alkali-deficient, Cr- and V-bearing

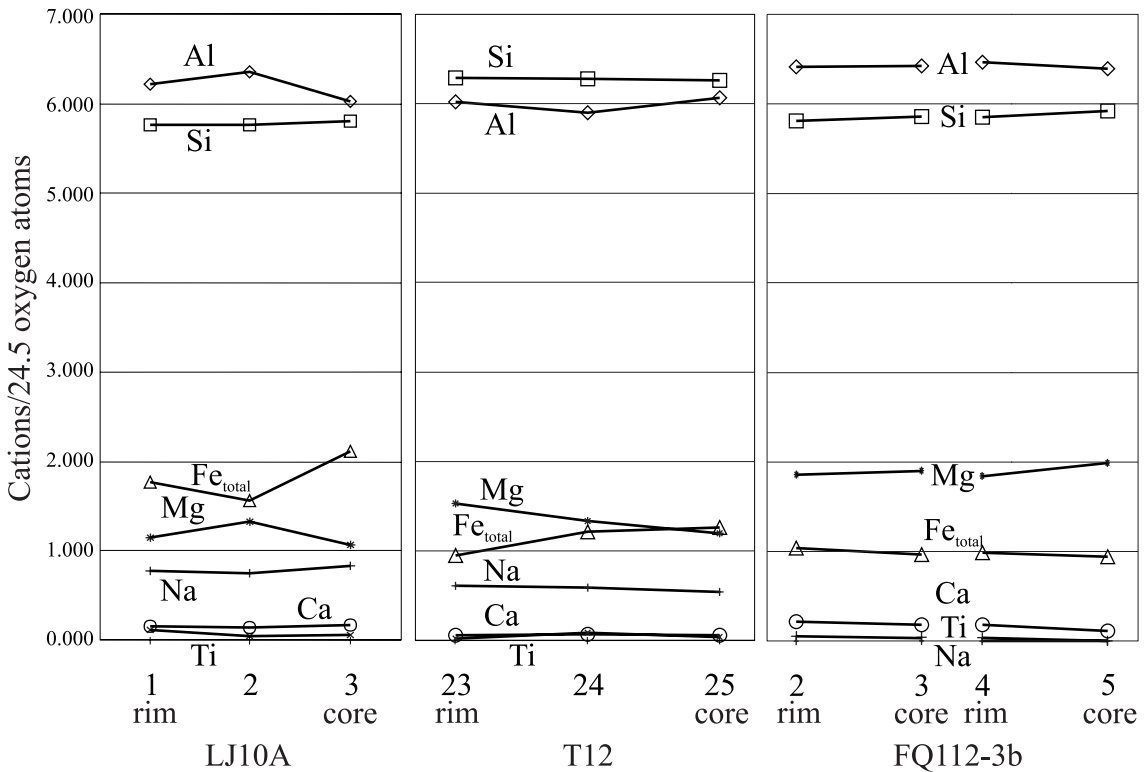
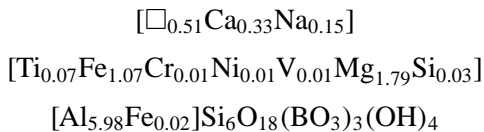


Fig. 6 – Variations of number of atoms per formula unit (apfu) from rim to core of tourmaline crystals in metachert (LJ10A – Tapera Grande), tourmalinite (T12 – Tapera Grande) and quartz vein (FQ112-3b – Quartzito).

tourmalines (Table II). The structural formula proposed for the FQ112-3a tourmaline is:



which corresponds to an intermediate composition between foitite (McDonald et al. 1993) and magnesiofoitite (Hawthorne et al. 1999).

RAMAN SPECTROSCOPY

Polished thin sections of tourmaline-rich metachert (LJ10) and tourmalinite (T12) from Tapera Grande, and a tourmaline-rich quartz vein (FQ-112-3a) from Quartzito were analyzed by Raman spectrometry. Raman spectra of schorl GRR#794 from Cahuilla Mountain (Riverside,

California) and a magnesiofoitite from Honshu (Japan) – available at the Mineral Spectroscopy Server of the California Institute of Technology (<http://minerals.gps.caltech.edu>) – are presented for comparison.

Peaks corresponding to tourmalines from LJ10 and T12 appear at 235-239 cm^{-1} , 360-367 cm^{-1} , and 635-700 cm^{-1} intervals (three consecutive peaks – Fig. 7.2a). According to Gasharova et al. (1997), these peaks are characteristic of G1 – intermediate between buergerite and schorl of the buergerite-schorl group. For tourmaline T12, peaks at 3228 and 3475 cm^{-1} were obtained (Fig. 7.2b), the former having no correspondence with schorl GRR#794 spectrum close to the OH region (3400-3800 cm^{-1} interval – Fig. 7.1b).

TABLE II

**XRF analyses of tourmalines from Tapera Grande and Quartzito.
Structural formulae calculated on 31 oxygen basis.**

Sample	SRT-2-97	SRT-3-99	FQ112-3A	Sample	SRT-2-97	SRT-3-99	FQ112-3A
SiO ₂	35.97	35.42	36.71	B	3.000	3.000	3.000
TiO ₂	0.90	0.69	0.56				
Al ₂ O ₃	28.84	29.10	30.84	Al _{total}	5.738	5.813	5.977
Cr ₂ O ₃	0.00	0.00	0.08	Si _{total}	6.070	6.002	6.035
FeO	13.35	13.81	7.95				
MnO	0.03	0.03	0.00	Si _T	6.000	6.000	6.000
MgO	4.22	4.18	7.31	Al _T	0.000	0.000	0.000
CaO	1.79	1.48	1.89				
Na ₂ O	1.44	1.78	0.47	Al _Z	5.738	5.813	5.977
K ₂ O	0.14	0.20	0.01	Fe ³⁺	0.262	0.187	0.023
V ₂ O ₅	0.02	0.04	0.09				
NiO	< d.l.	< d.l.	0.09	Al _Y	0.000	0.000	0.000
				Si _Y	0.070	0.002	0.035
	ppm	ppm	ppm	Ti	0.114	0.087	0.070
Ba	< 37	< 37	62	Fe _{total}	1.885	1.957	1.092
Ce	215	280	95	Fe ²⁺	1.622	1.770	1.070
Co	29	28	44	Cr	0.000	0.000	0.010
Cr	< 13	< 13	534	Ni	0.000	0.000	0.012
Cu	71	344	2323	V	0.001	0.003	0.006
Ga	59	65	45	Mn	0.004	0.004	0.000
La	< 28	< 28	64	Mg	1.061	1.056	1.791
Nb	38	27	85	Y _{total}	2.873	2.922	2.993
Nd	160	38	33				
Ni	< 3	< 3	705	Ca	0.324	0.269	0.333
Pb	< 3	< 3	< 3	Na	0.471	0.585	0.150
Rb	18	8	29	K	0.030	0.043	0.001
S	61	705	3207	X _{total}	0.825	0.897	0.484
Sc	< 14	77	44	[]	0.175	0.103	0.516
Sr	497	444	489				
Th	< 6	< 6	< 6	Total Cations	15.698	15.819	15.477
U	37	33	62				
V	138	211	488	R1	0.795	0.854	0.483
Y	127	57	55	R2	2.946	3.013	2.883
Zn	154	111	< 2	R3	5.889	5.929	6.070
Zr	459	130	232	Mg#	0.360	0.350	0.621

TABLE III
Stable oxygen and hydrogen isotope analyses for quartz and tourmalines
from Tapera Grande and Quartzito.

Sample		$\delta^{18}\text{O}_{\text{SMOW}}$ quartz (per mil)	$\delta^{18}\text{O}_{\text{SMOW}}$ tourmaline (per mil)	δD tourmaline (per mil)
LF-10B	metachert	13.9	12.9	-104
LJ-09	metachert	13.8	13.5	-103
SRT-2-96B	quartz vein	13.2	11.6	
SRT-3-99	quartz vein	12	12	-86
F-01(1B)-3,80m	metachert	12.8	11.6	
F-04-17,55m	metachert	12.7	11.5	
FQ-112-(3A)-18,40m	quartz vein	13.6	11.8	-102

Alkali-deficient tourmalines from Quartzito show peaks at 116, 214, 238, 365, 491, 698-702, 841 cm^{-1} in the 100-800 cm^{-1} interval (Fig. 7.4a), corresponding to G3V of the dravite-buergerite-uvite series of Gasharova et al. (1997), characterized by 0.30 \square_{X} and 0.28 Ti apfu. The peak found at 3578 cm^{-1} (Fig. 7.4b) is more likely coincident with schorl GRR#794 peaks in the OH region than with the peaks at 3632 and 3622 cm^{-1} presented by Béziat et al. (1999) as indication of vacancy at the X-site, but more refined work has to be carried out.

Peaks characteristic of the elbaite group (at 224 cm^{-1} , and at positions further than 707 cm^{-1}) were not observed in the spectrograms.

ISOTOPIC DATA

Table III presents $\delta^{18}\text{O}$ values obtained for quartz and tourmaline crystals from tourmaline-rich metachert and quartz veins, and corresponding δD values for tourmalines.

The values of $\delta^{18}\text{O}$ and δD for tourmalines are plotted in Figure 8, which shows that tourmalines from Tapera Grande and Quartzito have

isotopic signatures different from those for primary magmatic waters and igneous rocks, being closer to the compositions that correspond to sediment waters.

The values of $\delta^{18}\text{O}$ for quartz and tourmalines from tourmaline-rich quartz veins and metachert are similar, the isotope fractionation between the two minerals varying from 0 to 1.8 per mil. Entering these values in Kotzer's et al. (1993) empirical oxygen-isotope fractionation factor equation, an oxygen-isotope equilibration temperature of 580°C is obtained.

DISCUSSION

A wide range of tourmaline compositions is identified in the Morro da Pedra Preta Formation, from intermediate schorl-dravite with varying Al contents (tourmalines from metachert and quartz veins), intermediate schorl-dravite with varying Mg and Fe contents (tourmalines from tourmalinite), and Cr(-V)-bearing foitite-magnesiofoitite, which is characterized by high Mg contents and X-site deficiency (Quartzito quartz veins). Discrete variations of Mg, Fe_{total} , Al and Ca apfu are observed

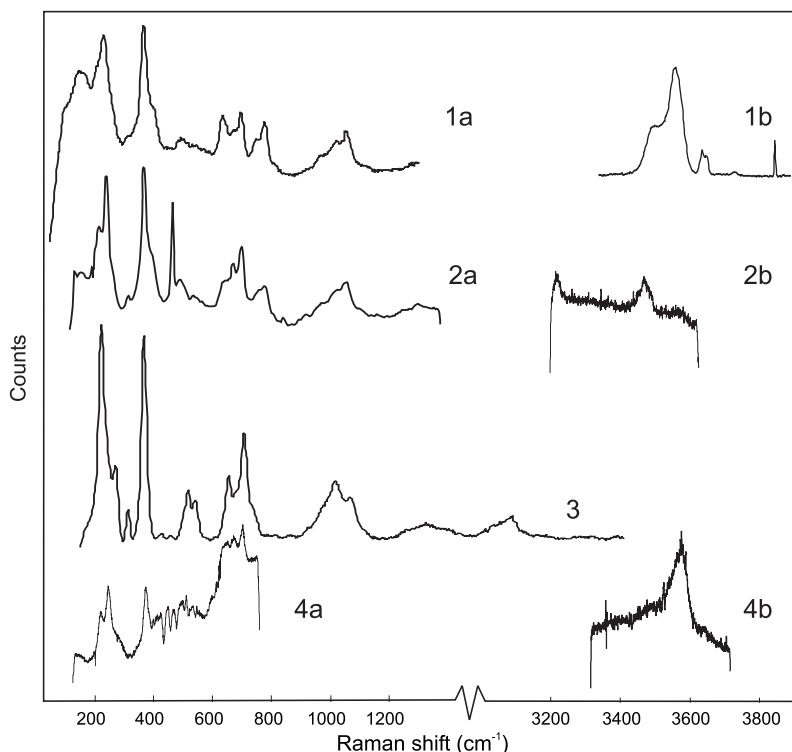


Fig. 7 – Raman spectra of (1) schorl GRR#794 from Cahuilla Mountain, Riverside (California); (2) tourmalines from metachert LJ10 and tourmalinite T12 (Tapera Grande); (3) magnesiofoitite from Honshu (Japan), and (4) tourmaline from quartz vein FQ112-3a (Quartzito).

TABLE IV

XRF analyses (Cr and V) of host rocks of Quartzito quartz veins.

Sample	Depth	Cr (ppm)	V (ppm)
FQ112-2	17.90 to 18.80 m	205	233
FQ112-43-1	43.45 to 43.40 m	76	235
FQ-112	44.00 to 44.80 m	557	191
F112-45-4	45.43 to 45.58 m	714	234
FQ112-47 (MgO = 15.96%)	47 m	74	136
FQ-112-48-1	48.15 to 48.30 m	711	224

in zoned crystals of intermediate schorl-dravite and foitite-magnesiofoitite, as well as variations of Na and Ti in the former and Cr (and V)

in the latter.

Compositional variations in growing tourmalines can be related to variations in environ-

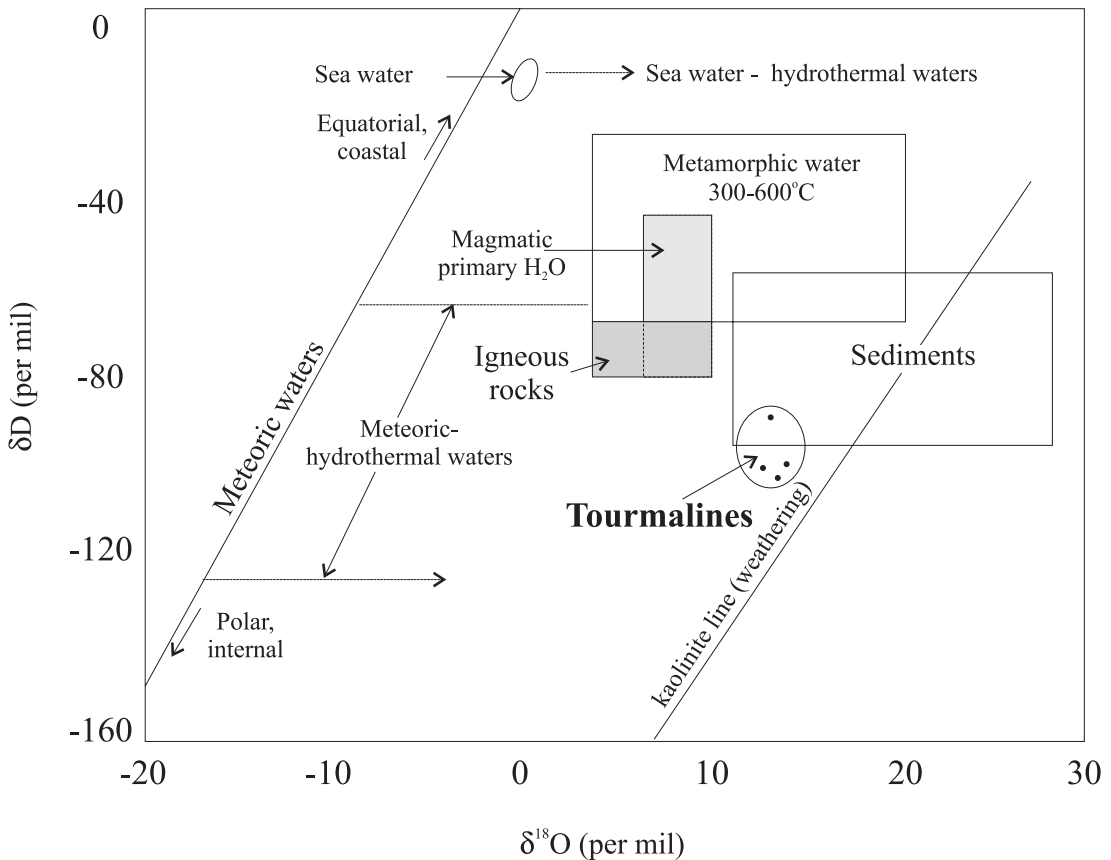


Fig. 8 – Representation of $\delta^{18}\text{O}$ and δD values obtained for tourmalines from Tapera Grande and Quartzito in Taylor's (1967) diagram for isotopic compositions of waters from several origins.

ment and metamorphic conditions and composition of circulating fluids, but once tourmaline is formed, it is stable under a wide range of physical-chemical conditions. Henry and Dutrow (1996) report the occurrence of tourmalines according to increasing metamorphic grades, showing that there is a correlation between Al, Ca and X-site-vacancy contents that apparently does not depend on metamorphism, but rather on the phases present. For example, in metapelites, aluminous, high-X-site-vacancy tourmalines coexist with aluminous minerals such as staurolite and sillimanite; there is an inverse correlation between Ca and X-site vacancy. On the other hand, tourmalines that grow

in low-Al metapelites contain lower values of X-site vacancy. In medium-grade metapelites and quartzites, tourmalines are intermediate schorl-dravite with variable Al and X-site-vacancy amounts. Although in this study tourmalines closely related to metamorphic minerals (such as those found in basic metatuffs and volcanic rocks) have not been analyzed, a certain correlation between Al and X-site vacancy contents is observed for the studied tourmalines from Tapera Grande and Quartzito.

Henry and Dutrow (1996) also stated that metamorphosed stratiform tourmalinites, typically associated with metapelites, metapsammites or meta-ironstones, are interpreted as be-

ing formed by early diagenesis of B-rich chemical precipitates, or by metasomatic modifications due to volcanic exhalations during sedimentation. Tourmalines from stratiform tourmalinites have several common chemical characteristics with tourmalines developed in metapsammites and metapelites, e.g., they can be peraluminous, coexisting with Al-saturated minerals such as sillimanite, or can be less aluminous if they coexist with less aluminous minerals. These findings agree with compositional variations obtained for Tapera Grande T12 tourmalinite.

Tourmaline, developed as a consequence of infiltration of B-bearing hydrothermal fluids, can have a wide range of compositions that depend on the compositions of the altering host rock and the invading fluid. This type of B metasomatism is commonly associated with a wide variety of precious metal deposits such as Au, Ag, Zn, U, and Mo. In the Quartzito area, scheelite, molybdenite, and sphalerite were identified in drillhole samples, associated with pyrite and chalcopyrite.

The tourmaline chemistry is dominated by the nature of the host rock, but in other cases tourmaline has a "mixed" chemical signature influenced by the chemistry of the fluids. When hydrothermal fluid becomes dominant, the B-rich fluids can lead to extensive tourmalinization. It is relatively selective in that B-rich fluids will preferentially tourmalinize rocks with the requisite Mg-Fe-Al constituents. In general these tourmalines tend to have compositions of schorl to intermediate schorl-dravite, but can exhibit considerable amount of X-site vacancy and substitution of Fe³⁺ (e.g. Cavarretta and Puxeddu 1990). This is the case of Quartzito tourmaline-bearing quartz veins, whose compositions were also affected by the host rock chem-

istry. In Table IV Cr and V contents obtained from XRF analyses of host rocks of Quartzito quartz veins are listed. Regarding Cr, the values obtained for Quartzito are, at present, the highest ones found in whole rock analyses of drill-hole samples of Tapera Grande and Quartzito. High V contents are found in a variety of rocks, especially those of sedimentary origin.

CONCLUSIONS

From the data here presented, it is concluded that:

- Tourmalines from Tapera Grande and Quartzito metachert and from Tapera Grande tourmalinite are intermediate schorl-dravite, of syngenetic origin, formed under submarine, sedimentary-exhalative conditions. Amphibolite-grade metamorphism did not strongly affect their compositions.
- Quartz veins that crosscut the Morro da Pedra Preta Formation not only contain intermediate schorl-dravite (Tapera Grande), but also alkali-deficient, Cr-(V)-bearing foitite-magnesiofoitite (Quartzito), which are characterized by higher Mg# values than those for intermediate schorl-dravite.
- Foitite-magnesiofoitite reflects the composition of the host rocks of Quartzito quartz veins, where fluid percolation along faults and fractures associated with the Sertãozinho Fault led to leaching of Cr (and V), and the crystallization of alkali-deficient, Cr-(V)-bearing tourmalines together with quartz.
- Raman spectroscopy also confirms the existence two distinct groups of tourmalines in Tapera Grande and Quartzito areas, and rules out the presence of elbaite. Should

magmatic/metasomatic origin be the case, schorlitic-elbaitic (Li and Al rich) compositions would be expected, according to e.g. Plimer (1986).

- Stable isotope data indicate sediments as fluid sources for the intermediate schorl-dravite and foitite-magnesiofoitite, ruling out a direct (post-)magmatic origin. $\delta^{18}\text{O}$ compositions for tourmalines and host metachert or quartz veins are very similar, suggesting that fluid equilibration occurred during crystallization of both minerals.
- In spite of the occurrence of granitic bodies intruding the Serra do Itaberaba Group, the studied tourmalines are not directly related to them. The same conclusion was drawn by Kassoli-Fournaraki and Michailidis (1994), when studying tourmaline-bearing quartz veins crosscutting metamorphic rocks in Macedonia (northern Greece). There is still the possibility, though, that granitic bodies could have been the heat source for circulating, reactive fluids.

ACKNOWLEDGMENTS

The authors wish to thank Prof. Anthony E. Fallick for making stable oxygen and hydrogen isotope analyses at the Scottish Universities Environmental Research Center (East Kilbride, UK) possible, and to São Paulo State Research Foundation FAPESP (Process numbers 98/05526-09 and 99/05792-03) for financial support. The authors are indebted to the anonymous referees for their helpful suggestions.

RESUMO

Na Formação Morro da Pedra Preta, seqüência vulcano-sedimentar do Grupo Serra do Itaberaba

(São Paulo, Brasil), turmalinas de composição intermediária schorl-dravita ocorrem em formação ferífera (incluindo turmalinito e metachert), metasedimentos, rochas cálcio-silicáticas e metabásicas a intermediárias.

A Formação Morro da Pedra Preta é cortada por veios de quartzo que contêm tanto schorl-dravita intermediária, como turmalinas com Cr e V deficientes em álcalis. A ocupação do sítio X é $\square_{0.51}\text{Ca}_{0.33}\text{Na}_{0.15}$, caracterizando-as como intermediárias aos membros extremos foitita e magnesiofoitita. Seus valores de Mg# são mais elevados do que aqueles da schorl-dravita intermediária.

A espectroscopia Raman também confirma a presença de dois grupos de turmalinas. Dados de isótopos estáveis indicam como fontes de fluídos águas de origem sedimentar, em detrimento a fluídos oriundos de fonte (pós-)magmática. As composições de $\delta^{18}\text{O}$ das turmalinas e quartzo dos veios são muito semelhantes, mostrando ter havido equilíbrio isotópico de fluídos durante sua cristalização.

Schorl-dravita intermediária formou-se em condições sedimentares-exalativas submarinas; sua composição não foi fortemente afetada pelo metamorfismo. Turmalinas mais jovens, de composição entre foitita-magnesiofoitita, refletem a composição das rochas hospedeiras dos veios de quartzo, sendo que os fluídos que percolaram falhas e fraturas lixiviaram Cr (e V), ocorrendo cristalização de turmalinas deficientes em álcalis com Cr (e V) em veios.

Palavras-chave: série schorlita-dravita, foitita-magnesiofoitita, Grupo Serra do Itaberaba, Formação Morro da Pedra Preta.

REFERENCES

- BELJAVSKIS P, JULIANI C, GARDA GM, XAVIER RP AND BETTENCOURT JS. 1999a. Overview

- of the gold mineralization in the metavolcanic-sedimentary sequence of the Serra do Itaberaba Group – São Paulo – Brazil. In: STANLEY CJ ET AL. (Ed.), *Mineral Deposits: Processes to Processing*, v.1, Rotterdam/Brookfield: Balkema, p. 151-153.
- BELJAVSKIS P, GARDA GM AND SAYEG IJ. 1999b. Application of SEM in the study of gold mineralizations in the Morro da Pedra Preta Formation, Grupo Serra do Itaberaba – São Paulo, Brazil. *Acta Microscopica* 8 (Supplement A): 125-126.
- BÉZIAT D, BOURGES F, DEBAT P, FUCHS Y, LOMPO M, MARTIN F, NIKIÉMA S AND TOLLON F. 1999. The Guibaré and Fété Kolé gold-bearing tourmaline-quartz veins in the Birimian Greenstone belts of Burkina Faso. *Canadian Mineralogist* 37: 575-591.
- BONE Y. 1988. The geological setting of tourmalinite at Rum Jungle, N.T., Australia – genetic and economic implications. *Mineral Deposita* 23: 34-41.
- CAVARRETTA G AND PUXEDDU M. 1990. Schorl-draivite-ferridraivite tourmalines deposited by hydrothermal magmatic fluids during early evolution of the Larderello geothermal field, Italy. *Econ Geol* 85: 1236-1251.
- FALLICK AE, McCONVILLE P, BOYCE AJ, BURGESS R AND KELLEY SP. 1992. Laser microprobe stable isotope measurements on geological materials: some experimental considerations (with special reference to $\delta^{34}\text{S}$ in sulphides). *Chem Geol* 101: 53-61.
- GARDA GM, BELJAVSKIS P AND SAYEG IJ. 1999. Gold mineralization in the Quartzito area, the Serra do Itaberaba Group – São Paulo, Brazil. *Acta Microscopica* 8 (Supplement A): 127-128.
- GARDA GM, BELJAVSKIS P, JULIANI C AND BOYCE AJ. 2002. Sulfur stable isotope signatures of the Morro da Pedra Preta Formation, Serra do Itaberaba Group, São Paulo State, Brazil. *Geochimica Brasiliensis* (in press).
- GASHAROVA B, MIHAILOVA B AND KONSTANTINOV L. 1997. Raman spectra of various types of tourmaline. *Eur J Mineral* 9: 935-940.
- HAWTHORNE FC AND HENRY DJ. 1999. Classification of the minerals of the tourmaline group. *Eur J Mineral* 11: 201-215.
- HAWTHORNE FC, SELWAY JB, KATO A, MATSUBARA S, SHIMIZU M, GRICE, JD AND VAJDAK J. 1999. Magnesiofoitite, $[(\text{Mg}_2\text{Al})\text{Al}_6(\text{Si}_6\text{O}_{18})(\text{BO}_3)_3(\text{OH})_4]$, a new alkali-deficient tourmaline. *Can Mineral* 37: 1439-1443.
- HENRY DJ AND DUTROW BL. 1996. Metamorphic tourmaline and its petrologic applications. In: GREW ES AND ANOVITZ LM (Ed.), *Boron – Mineralogy, petrology and geochemistry*. *Rev Mineral* 33: 503-557.
- HENRY DJ AND GUIDOTTI CV. 1985. Tourmaline as a petrogenetic indicator mineral: an example from the staurolite-grade metapelites of NW Maine. *Am Mineral* 70: 1-15.
- JANASI V AND ULBRICH HHGJ. 1991. Late Proterozoic granitoid magmatism in the state of São Paulo, southeastern Brazil. *Precambrian Res* 51: 351-374.
- JULIANI C. 1993. Geologia, petrogênese e aspectos metalogenéticos dos grupos Serra do Itaberaba e São Roque na região das Serras do Itaberaba e da Pedra Branca, NE da cidade de São Paulo, SP. São Paulo, 684p. (Doctorate Thesis. Instituto de Geociências da USP).
- JULIANI C AND BELJAVSKIS P. 1995. Revisão da litoestratigrafia da faixa São Roque/Serra do Itaberaba (SP). *Revista do IG* 16(1/2): 33-58.
- JULIANI C, HACKSPACKER P, DANTAS EL AND FETTER AH. 2000. The Mesoproterozoic volcano-sedimentary Serra do Itaberaba Group of the central Ribeira Belt, São Paulo State, Brazil: implications for the age of the overlying São Roque Group. *Rev Bras Geoc* 30: 82-86.
- KASSOLI-FOURNARAKI A AND MICHAELIDIS K. 1994. Chemical composition of tourmaline in quartz veins from Nea Roda and Thasos areas in Macedonia, Northern Greece. *Can Mineral* 32: 607-615.

- KING RW AND KERRICH R. 1989. Chromian dravite associated with ultramafic-rock-hosted Archean lode gold deposits, Timmins-Porcupine District, Ontario. *Can Mineral* 27: 419-426.
- KOTZER TG, KYSER TK, KING RW AND KERRICH R. 1993. An empirical oxygen- and hydrogen-isotope geothermometer for quartz-tourmaline and tourmaline-water. *Geochim Cosmochim Acta* 57: 3421-3426.
- MCDONALD DJ, HAWTHORNE FC AND GRICE JD. 1993. Foitite, $\square[(\text{Fe}_2^{2+}(\text{Al}, \text{Fe}^{3+}))\text{Al}_6\text{Si}_6\text{O}_{18}(\text{BO}_3)_3(\text{OH})_4]$, a new alkali-deficient tourmaline: Description and crystal structure. *Am Mineral* 78: 1299-1303.
- PLIMER IR. 1983. The association of tourmaline-bearing rocks with mineralization at Broken Hill, N.S.W. *Proc Ann Aus Inst Min Met Conf*, p. 157-176.
- PLIMER IR. 1986. Tourmalinites from the Golden Dyke Dome, Northern Australia. *Mineral Deposita* 21: 263-270.
- PLIMER IR. 1987. The association of tourmaline with stratiform scheelite deposits. *Mineral Deposita* 22: 282-291.
- PLIMER IR. 1988. Tourmalines associated with Australian Proterozoic submarine exhalative ores. In: FRIEDRICH GH AND HERZIG PM. (Eds.) *Base metal sulfide deposits in sedimentary and volcanic environments*. Berlin: Springer-Verlag, p. 255-283.
- SLACK JF. 1982. Tourmaline in Appalachian-Caledonian massive sulphide deposits and its exploration significance. *Trans Instn Min Metall* 91: B81-B89.
- SLACK JF. 1996. Tourmaline associations with hydrothermal ore deposits. In: GREW ES AND ANOVITZ LM (Ed.), *Boron – Mineralogy, petrology and geochemistry*. *Rev Mineral* 33: 559-643.
- SLACK JF, HERRIMAN N, BARNES RG AND PLIMER IR. 1984. Stratiform tourmalines in metamorphic terranes and their geologic significance. *Geology* 12: 713-716.
- TAYLOR BE AND SLACK JF. 1984. Tourmalines from the Appalachian-Caledonian massive sulfide deposits: textural, chemical, an isotopic relationships. *Econ Geol* 79: 1703-1726.
- TAYLOR JR HP. 1967. Oxygen isotope studies of hydrothermal mineral deposits. In: BARNES HL (Ed.), *Geochemistry of hydrothermal ore deposits*. Holt, Rinehart and Winston, 670p.
- WILLNER AP. 1992. Tourmalines from the stratiform peraluminous metamorphic suite of the Central Namaqua Mobile Belt (South Africa). *Mineral Deposita* 27: 304-313.
- YAVUZ F. 1997. TOURMAL: Software package for tourmaline, tourmaline-rich rocks and related ore deposits. *Computers and Geosciences* 23: 947-959.